6th European Conference on Computational Mechanics (ECCM 6)
7th European Conference on Computational Fluid Dynamics (ECFD 7)
1115 June 2018, Glasgow, UK

AN ISOGEOMETRIC SOLID-SHELL FORMULATION OF THE KOITER METHOD FOR BUCKLING AND INITIAL POST-BUCKLING ANALYSIS OF COMPOSITE SHELLS

Leonardo Leonetti[1], Domenico Magisano[1], Francesco Liguori[1] and Giovanni Garcea[1]

[1] Dipartimento di Ingegneria Informatica, Modellistica, Elettronica e Sistemistica Università della Calabria, 87036, Rende (Cosenza), Italy, giovanni.garcea@unical.it

Key words: Buckling, isogeometric analysis, composite shells, Koiter method

Abstract. Numerical formulations of the Koiter theory allow the efficient prediction, through a reduced order model, of the behavior of shell structures when failure is dominated by buckling. In this work, we propose an isogeometric version of the method based on a solid-shell model. A NURBS-based interpolation is employed on the middle surface of the shell to accurately describe the geometry and the high continuity typical of the displacement field in buckling problems and to directly link the CAD model to the structural one. A linear interpolation is then adopted through the thickness together with a modified generalized constitutive matrix, which allows us to easily eliminate thickness locking and model multi-layered composites. Reduced integration schemes, which take into account the continuity of the shape functions, are used to avoid interpolation locking and make the integration faster. A Mixed Integration Point strategy makes it possible to transform the displacement model into a mixed (stress-displacement) one, required by the Koiter method to obtain accurate predictions, without introducing stress interpolation functions. The result is an efficient numerical tool for buckling and initial post-buckling analysis of composite shells, characterized by a low number of DOFs and integration points and by a simple and quick construction of the reduced order model.

1 INTRODUCTION

The failure of composite shells often occurs because of buckling phenomena which make them sensitive to material, geometrical and load imperfections [1]. Thousands of equilibrium path evaluations can be required in order to detect the worst imperfection case in terms of failure load. Furthermore, the stacking sequence has proven to strongly affect the buckling and post-buckling response of the shells and the design of an optimal layup can significantly increase the load-carrying capability. Consequently, the need for an optimization process leads to a further computational burden and requires more efficient tools of analysis and design. For these reasons, a great amount of research has focused on developing reduced order models (ROMs) based on the finite element (FE) implementation [2, 3] of the Koiter theory of elastic stability, capable of furnishing, with an acceptable

computational cost, an accurate prediction [1] of the limit load value and the initial post-critical behaviour for a very large number of imperfections. A solid-shell FE model [4] is particularly convenient for the construction of the ROM, since it allows us to avoid the use of finite rotations. Although a large number of locking free linear solid-shell elements are available, their behavior is not sufficiently accurate when modeling curved geometry and, as a consequence, a fine discretization is required. An interesting alternative is given by the isogeometric analysis (IGA) [5] based on NURBS shape functions. IGA seems very attractive in particular in buckling problems, where a highly continuous solution is often expected [6, 7, 1]. It has been shown in [3] that the Koiter method requires a mixed formulation in order to avoid a locking phenomenon in the evaluation of the fourth-order coefficients of the reduced system of equations and to increase the range of validity of the ROM, which gets worse in displacement formulations when the slenderness of the structure increases [3] and the pre-buckling path exhibits even small nonlinearities. This aspect can also be observed in path-following analyses [3, 4, 8] where displacement formulations lead to a slow convergence rate of the Newton scheme when slender structures are analyzed. In Koiter analysis this phenomenon is much more evident because the equilibrium path is directly extrapolated using the ROM, and an equilibrium error is not corrected by an iterative scheme, so affecting the accuracy of the method. On the contrary mixed formulations avoid this drawback because the stresses are directly extrapolated. Furthermore, the joint use of a Green-Lagrange strain measure and of a mixed Hellinger-Reissner variational formulation [2, 3], leads to a $3rd$ order polynomial dependence of the strain energy on the discrete DOFs with the consequence of the zeroing of all the fourth order strain energy variations. In this work, we propose an isogeometric numerical formulation of the Koiter theory for the analysis of composite shells which exploits the advantages of a solid-shell model. A linear through-the-thickness interpolation is considered for geometry and displacements. The nonlinear model is based on a Total-Lagrangian formulation with the use of the Green-Lagrange strain measure. Inspired by the FE approach proposed by Sze [4], the Green-Lagrange strains are linearized along the thickness direction, allowing the definition of a modified generalized constitutive matrix which effectively eliminates thickness locking and leads to accurate predictions for multi-layered composites, without introducing additional through-the-thickness DOFs. The displacement field and the geometry are rewritten in terms of semi-sum and semi-difference of the top and bottom surface quantities. The model so obtained is described by middle surface coordinates only, allowing us to interpolate geometry and displacements using bivariate NURBS of generic order and continuity. Each control point is equipped with six DOFs but, in contrast to traditional shell models, only displacement DOFs are employed. Different patch-wise reduced integration rules [9, 10], previously proposed for linear analysis, are investigated in stability problems with the aim of eliminating interpolation lockings and increasing the computational efficiency when C^1 and C^2 NURBS are adopted. To obtain the mixed description of the problem, required by the Koiter formulation, the Mixed Integration Point (MIP) strategy, recently proposed in [8] for finite element path-following analyses, is here extended to the proposed isogeometric Koiter analysis.

2 KOITER IGA USING MIXED INTEGRATION POINTS

2.1 The nonlinear model and the numerical integration

We consider a slender hyperelastic structure subject to conservative loads $p[\lambda]$ proportionally increasing with the amplifier factor λ. The equilibrium is expressed by the virtual work equation

$$\Phi[u]' \, \delta u - \lambda \hat{p} \, \delta u = 0 \quad , \quad u \in \mathcal{U} \; , \; \delta u \in \mathcal{T} \tag{1}$$

where $u \in \mathcal{U}$ is the field of configuration variables, $\Phi[u]$ denotes the strain energy, $\mathcal{T}$ is the tangent space of $\mathcal{U}$ at u and a prime is used to express the Frechèt derivative with respect to u. We assume that $\mathcal{U}$ will be a linear manifold so that its tangent space $\mathcal{T}$ will be independent of u. When a mixed format is adopted the configuration variables u collect both displacement and stress fields. The displacement based IGA formulation previously presented allows us to express the strain energy of the element as a sum of element contributions $\Phi[u] \equiv \sum_e \Phi_e[\mathbf{d}_e]$

$$\Phi_e[\mathbf{d}_e] \equiv \int_{\Omega_e} \left(\frac{1}{2} \boldsymbol{\varepsilon}^T \mathbf{C}_\epsilon \boldsymbol{\varepsilon} \right) d\Omega_e \tag{2}$$

where Ω_e is the element domain and a numerical integration is usually adopted. The shell is modeled using the isogeometric solid-shell model proposed in [11]. The d-dimensional target space of order p and regularity r, labeled as $\mathcal{S}_r^p$, is exactly integrated by a number of $\approx ((p-r)/2)^d$ integration points per element, distributed over the patch, significantly lower than in standard Gauss quadrature rules. Their positions and weights are not equal for each element, but are evaluated, once and for all, in a pre-processing phase and depend on r, p and patch mesh [10, 9]. They also open up new possibilities for patch-wise reduced integration schemes. In fact p and r can be selected by the user and are not required to be those for the exact integration of the problem space. If the integration space presents spurious modes, a certain number of quadrature points are added near the boundary elements in order to remove them and the approximation space is said to be over-integrated and labeled as $\bar{\mathcal{S}}_r^p$ [10, 9]. The number of integration points n can be different element-by-element and the strain energy can be evaluated as

$$\Phi_e[\mathbf{d}_e] \equiv \frac{1}{2} \sum_{g=1}^{n} \boldsymbol{\varepsilon}_g[\mathbf{d}_e]^T \mathbf{C}_g \boldsymbol{\varepsilon}_g[\mathbf{d}_e] \; w_g \tag{3}$$

where subscript g denotes quantities evaluated at the integration point $[\xi_g, \eta_g]$, w_g is the product of the corresponding weight and the determinant of the Jacobian matrix $\mathbf{J}$ evaluated at the integration point and $\mathbf{C}_g$ is $\mathbf{C}_\epsilon$ at the integration point.

2.2 The Koiter method using mixed integration points

The fundamental idea of the MIP strategy [8] is to relax the constitutive equations at the level of each integration point. This is made by rewriting the strain energy in a

pseudo Hellinger-Reissner form on the element

$$\Phi_e[\mathbf{u}_e] \equiv \sum_{g=1}^{n} \left(\boldsymbol{\sigma}_g^T \boldsymbol{\varepsilon}_g[\mathbf{d}_e] - \frac{1}{2} \boldsymbol{\sigma}_g^T \mathbf{C}_g^{-1} \boldsymbol{\sigma}_g \right) w_g \tag{4}$$

where the stresses at each integration point $\boldsymbol{\sigma}_g$ are now independent variables being

$$\mathbf{u}_e = \begin{bmatrix} \boldsymbol{\sigma}_1 \\ \vdots \\ \boldsymbol{\sigma}_n \\ \mathbf{d}_e \end{bmatrix} \tag{5}$$

The Koiter method is based on a third order Taylor expansion of Eq.(1), in λ and the modal amplitudes α_i [1, 2]. Letting $u_i \in \mathcal{T}$ be a generic variation of the displacement field and denoting with a bold symbol the discrete FEM counterpart of the continuum quantities, and referring to the solid-shell finite element model presented in [2], the reduced model construction for the *perfect structure* consists of the following steps.

1. The fundamental path is evaluated as

$$\mathbf{u}^f[\lambda] = \mathbf{u}_0 + \lambda \hat{\mathbf{u}} \quad , \quad \mathbf{K}_0 \, \hat{\mathbf{u}} = \mathbf{f} \quad , \quad \mathbf{K}_0 \equiv \mathbf{K}[\mathbf{u}_0] \tag{6a}$$

   where $\mathbf{K}_0$ and $\mathbf{f}$ are obtained from the following energy equivalence

$$\mathbf{u}_1^T \mathbf{K}_0 \mathbf{u}_2 := \Phi_0'' u_1 u_2 \qquad \mathbf{u}_1^T \mathbf{f} = p \; u_1.$$

   and requires the solution of a linear system to evaluate the initial path tangent $\hat{\mathbf{u}}$. A subscript will denote, from now on, the point in which the quantities are evaluated, i.e. $\Phi_0'' \equiv \Phi''[u_0]$ and so on.

2. The buckling modes and loads are obtained from the linearized critical condition consisting of the eigenvalue problem

$$\mathbf{K}[\lambda]\dot{\mathbf{v}} \equiv (\mathbf{K}_0 + \lambda \mathbf{K}_1[\hat{\mathbf{u}}])\dot{\mathbf{v}} = \mathbf{0} \tag{6b}$$

   where $\mathbf{K}_1$ is obtained from the following energy equivalence

$$\mathbf{u}_1^T \mathbf{K}_1 \mathbf{u}_2 = \Phi_0''' \hat{u} u_1 u_2.$$

3. The $(m \times (m+1))/2 + 1$ quadratic corrective FE vectors $\mathbf{w}_{ij}$, $\hat{\hat{\mathbf{w}}}$ are obtained by the solution of the linear systems

$$\begin{aligned} &\mathbf{K}_b \hat{\hat{\mathbf{w}}} + \hat{\hat{\mathbf{f}}} + \sum_{\mathbf{k=1}}^{\mathbf{m}} \mathbf{c_k} \hat{\mathbf{f}}_\mathbf{k} = \mathbf{0} \qquad \text{with} \quad c_k = \dot{\mathbf{v}}_k^T \hat{\hat{\mathbf{f}}} \\ &\mathbf{K}_b \mathbf{w}_{ij} + \mathbf{f}_{ij} + \sum_{k=1}^{m} c_k \hat{\mathbf{f}}_k = \mathbf{0} \quad \text{with} \quad c_k = \dot{\mathbf{v}}_k^T \mathbf{f}_{ij} \end{aligned} \tag{6c}$$

in which $\mathbf{K}_b \equiv \mathbf{K}_0 + \lambda_b \mathbf{K}_1$, $\hat{\mathbf{f}}_k = \mathbf{K}_1 \dot{\mathbf{v}}_k$, λ_b is a reference value of the bifurcation cluster, usually the first buckling load and $\mathbf{f}_{ij}, \mathbf{f}_{00}$ are defined as a function of modes $\dot{\mathbf{v}}_i$ and $\hat{\mathbf{u}}$ by the energy equivalences

$$\delta \mathbf{w}^T \mathbf{f}_{ij} = \Phi''' \dot{v}_j \dot{v}_j \delta w \qquad \delta \mathbf{w}^T \hat{\hat{\mathbf{f}}} = \Phi''' \hat{u}^2 \delta w$$

4. The construction of the reduced system of equations

$$\begin{aligned} r_k[\lambda, \alpha_i] \equiv \mu_k[\lambda] + (\lambda_k - \lambda)\alpha_k - \frac{1}{2}\lambda^2 \sum_{i=1}^{m} \alpha_i \mathcal{C}_{ik} + \frac{1}{2} \sum_{i,j=1}^{m} \alpha_i \alpha_j \mathcal{A}_{ijk} \\ + \frac{1}{6} \sum_{i,j,h=1}^{m} \alpha_i \alpha_j \alpha_h \mathcal{B}_{ijhk} = 0, \quad k = 1 \cdots m \end{aligned} \tag{6d}$$

is carried out by evaluating the energy terms for $i, j, h, k = 1 \cdots m$, being $\Phi''_b u_1 u_2 = (\Phi''_0 + \lambda_b \Phi''' \hat{u}) u_1 u_2 \quad \forall u_1, u_2$ as sum of element contributions

$$\begin{aligned} \mathcal{A}_{ijk} =& \Phi''' \dot{v}_i \dot{v}_j \dot{v}_k \qquad \mathcal{C}_{ik} = \Phi''_b \hat{\hat{w}} w_{ik} \\ \mathcal{B}_{ijhk} =& -\Phi''_b (w_{ij} w_{hk} + w_{ih} w_{jk} + w_{ik} w_{jh}) \\ \mu_k[\lambda] =& \frac{1}{2} \lambda^2 \Phi''' \hat{u}^2 \dot{v}_k. \end{aligned}$$

The evaluation of the equilibrium path, to be repeated for each additional imperfection, is obtained by solving the modified reduced system

$$r_k[\lambda, \alpha_i] + \tilde{\mu}_k[\lambda, \alpha_i] = 0$$

where $\tilde{\mu}_k$ represents the effect of the imperfection, and can be evaluated as in [1].

2.3 Strain energy variations using mixed integration points

In the following $\mathbf{u}_{ig} = \{\boldsymbol{\sigma}_{ig}, \mathbf{d}_{ie}\}$ will denote the vector representation on the integration point g of u_i. The first variation of (4) is

$$\Phi'_e u_1 = \sum_{g=1}^{n} \begin{bmatrix} \boldsymbol{\sigma}_{1g} \\ \mathbf{d}_{1e} \end{bmatrix}^T \begin{bmatrix} \mathbf{s}_{g\sigma} \\ \mathbf{s}_{gd} \end{bmatrix} w_g \quad \text{with} \quad \begin{cases} \mathbf{s}_{g\sigma} \equiv \boldsymbol{\varepsilon}_g[\mathbf{d}_e] - \mathbf{C}_g^{-1} \boldsymbol{\sigma}_g \\ \mathbf{s}_{gd} \equiv \mathbf{B}_g[\mathbf{d}_e]^T \boldsymbol{\sigma}_g. \end{cases} \tag{7a}$$

and $\mathbf{B}_g[\mathbf{d}_e] = \mathbf{L}_g + \mathbf{Q}_g[\mathbf{d}_e]$. The second variation of (4) is

$$\Phi''_e u_1 u_2 = \sum_{g=1}^{n} \left\{ \boldsymbol{\sigma}_{1g}^T \mathbf{B}_g[\mathbf{d}_e] \mathbf{d}_{2e} + \boldsymbol{\sigma}_{2g}^T \mathbf{B}_g[\mathbf{d}_e] \mathbf{d}_{1e} + \boldsymbol{\sigma}_g^T \mathbf{Q}_g[\mathbf{d}_{1e}] \mathbf{d}_{2e} \right\} w_g. \tag{7b}$$

Letting $\varepsilon^Q_{gk} = \mathbf{d}_{1e}^T \boldsymbol{\Psi}_{gk} \mathbf{d}_{2e}$ the kth component of vector $\mathbf{Q}_g[\mathbf{d}_{1e}]\mathbf{d}_{2e}$ we have

$$\boldsymbol{\sigma}_g^T \mathbf{Q}_g[\mathbf{d}_{1e}]\mathbf{d}_{2e} \equiv \sum_k \sigma_{gk} \, \varepsilon^Q_{gk} = \mathbf{d}_{1e}^T \boldsymbol{\mathcal{G}}[\boldsymbol{\sigma}_g] \mathbf{d}_{2e} \quad \text{with} \quad \boldsymbol{\mathcal{G}}[\boldsymbol{\sigma}_g] = \sum_k \sigma_{gk} \boldsymbol{\Psi}_{gk}. \tag{7c}$$

In matrix form the second variation of (4), letting $\boldsymbol{\mathcal{G}}_g \equiv \boldsymbol{\mathcal{G}}_e[\boldsymbol{\sigma}_g]$, becomes

$$\Phi''_e u_1 u_2 = \sum_{g=1}^{n} \begin{bmatrix} \boldsymbol{\sigma}_{1g} \\ \mathbf{d}_{1e} \end{bmatrix}^T \begin{bmatrix} -\mathbf{C}_g^{-1} & \mathbf{B}_g \\ \mathbf{B}_g^T & \boldsymbol{\mathcal{G}}_g \end{bmatrix} \begin{bmatrix} \boldsymbol{\sigma}_{2g} \\ \mathbf{d}_{2e} \end{bmatrix} w_g = \sum_g \mathbf{u}_{1g}^T \mathbf{K}_g \mathbf{u}_{2g}. \tag{7d}$$

The second variation can also be written in vector form introducing the *incremental force vector* so defined

$$\Phi''_e u_1 u_2 = \sum_g \mathbf{u}_{1g}^T \mathbf{s}'_g[\mathbf{u}_{2g}] \quad \text{with} \quad \mathbf{s}'_g[\mathbf{u}_{2g}] \equiv \begin{bmatrix} -\mathbf{C}_g^{-1}\boldsymbol{\sigma}_{2g} + \mathbf{B}_g \mathbf{d}_{2e} \\ \mathbf{B}_g^T \boldsymbol{\sigma}_{2g} + \boldsymbol{\mathcal{G}}_g \mathbf{d}_{2e} \end{bmatrix} \tag{7e}$$

The third variation of the strain energy is

$$\Phi''_e u_1 u_2 u_3 = \sum_{g=1}^{n} \left\{ \boldsymbol{\sigma}_{1g}^T \mathbf{Q}_g[\mathbf{d}_{3e}]\mathbf{d}_{2e} + \boldsymbol{\sigma}_{2g}^T \mathbf{Q}_g[\mathbf{d}_{3e}]\mathbf{d}_{1e} + \boldsymbol{\sigma}_{3g}^T \mathbf{Q}_g[\mathbf{d}_{1e}]\mathbf{d}_{2e} \right\} w_g \tag{7f}$$

that can also be written in vector form introducing the *secondary force vector* as

$$\Phi'''_e \delta u_1 \delta u_2 \delta u_3 = \sum_g \mathbf{u}_{1g}^T \mathbf{s}''_g[\mathbf{u}_{2g}, \mathbf{u}_{3g}] \quad \text{with} \quad \mathbf{s}''_g[\mathbf{u}_{2g}, \mathbf{u}_{3g}] \equiv \begin{bmatrix} \mathbf{Q}_g[\mathbf{d}_{3e}]\mathbf{d}_{2e} \\ \mathbf{Q}_g[\mathbf{d}_{3e}]^T \boldsymbol{\sigma}_{2g} + \boldsymbol{\mathcal{G}}_g[\boldsymbol{\sigma}_{3g}]\mathbf{d}_{2e} \end{bmatrix} \tag{7g}$$

3 NUMERICAL RESULTS

3.1 Composite curved panel under compression

The first test regards a curved panel under compression whose geometry, loads, and boundary conditions are depicted in Fig.1. The material properties can be found in Table 1. Two different layups are considered: $[0]_6$ and $[45, -45, 0]_s$. The lamination significantly influences the shape of the buckling modes as illustrated in Fig.2. This is confirmed by Tables 2, 3, 4 and 5 which show the convergence of the first 4 linearized buckling loads. The high continuity together with the exact representation of the geometry leads to very good results with all the integration strategies. Again, however, the $\bar{S}_0^2$ for C_1 and S_1^4 and $\bar{S}_1^3$ for C_2 represent the best choices in terms of accuracy and efficiency. The study of the initial post-buckling behavior of the panel is carried out considering the presence of a geometrical imperfection $\tilde{e}$ that is a combination of the first and the second buckling modes. In particular, it is the difference between them scaled in order to obtain $\|\tilde{e}\|_\infty = 0.1t$. The Koiter solution is evaluated using a ROM based on the first two buckling modes only, since the higher ones are far from the first two, and it is compared with reference paths. For both the layups, the initial post-buckling exhibits a limit load as shown in Fig.3 and Fig.4 for $[0]_6$ and in Fig.5 and 6 for $[45, -45, 0]_s$. C_1-$\bar{S}_0^2$, C_2-$\bar{S}_1^3$ and C_2-S_1^4 are the best performing strategies, providing a good estimate of the limit loads with a 8×8 mesh, which became practically exact using a 16×16 mesh.

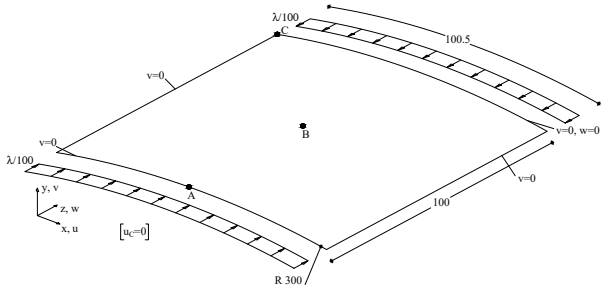

Figure 1: Composite curved panel: geometry and boundary conditions.

E_{11}	$E_{22} = E_{33}$	$\nu_{12} = \nu_{13}$	ν_{23}	$G_{12} = G_{13}$	G_{23}
30.6	8.7	0.29	0.5	3.24	2.9

Table 1: Composite curved panel: material properties.

4 elm.				8 elm.				16 elm.			
$\bar{S}_0^2$	S_0^3	S_0^4	ANS	$\bar{S}_0^2$	S_0^3	S_0^4	ANS	$\bar{S}_0^2$	S_0^3	S_0^4	ANS
1.053	1.055	1.078	1.042	1.002	0.998	1.020	1.008	0.995	0.995	0.998	0.996
1.158	1.424	1.694	1.177	1.005	1.008	1.069	1.018	0.996	0.998	1.003	0.997
1.259	1.609	$*$	1.299	1.009	1.035	1.124	1.039	1.003	1.004	1.012	1.003
1.408	1.746	$*$	1.396	1.007	1.061	1.213	1.067	1.003	1.005	1.020	1.004

$* > 2$

Table 2: Composite curved panel: first 4 normalized buckling loads for $[0]_6$ with C_1 interpolation.

4 elm.				8 elm.				16 elm.			
$\bar{S}_0^2$	S_0^3	S_0^4	ANS	$\bar{S}_0^2$	S_0^3	S_0^4	ANS	$\bar{S}_0^2$	S_0^3	S_0^4	ANS
1.096	1.144	1.263	1.165	1.016	1.018	1.095	1.054	1.001	1.002	1.015	1.004
1.082	1.201	1.656	1.106	1.013	1.010	1.078	1.036	0.998	0.999	1.011	1.001
1.080	1.346	$*$	1.333	1.007	1.010	1.157	1.061	0.998	0.999	1.010	0.999
1.235	1.456	$*$	1.848	1.035	1.073	1.228	1.119	1.003	1.012	1.049	1.011

$* > 2$

Table 3: Composite curved panel: first 4 normalized buckling loads for $[45, -45, 0]_s$ with C_1 interpolation.

4 elm.			8 elm.			16 elm.		
$\bar{S}_1^3$	S_1^4	S_1^6	$\bar{S}_1^3$	S_1^4	S_1^6	$\bar{S}_1^3$	S_1^4	S_1^6
0.995	1.034	1.031	1.001	1.005	1.004	1.001	1.002	1.001
1.000	1.013	1.073	1.001	1.004	1.003	1.001	1.001	1.001
1.008	1.063	1.132	1.003	1.008	1.007	1.002	1.003	1.003
1.014	1.104	1.210	1.004	1.009	1.010	1.002	1.003	1.003

Table 4: Composite curved panel: first 4 normalized buckling loads for $[0]_s$ with C_2 interpolation.

4 elm.			8 elm.			16 elm.		
$\bar{S}_1^3$	S_1^4	S_1^6	$\bar{S}_1^3$	S_1^4	S_1^6	$\bar{S}_1^3$	S_1^4	S_1^6
0.995	1.097	1.110	1.006	1.014	1.018	1.002	1.005	1.004
1.014	1.044	1.068	1.006	1.012	1.015	1.001	1.003	1.003
1.002	1.121	1.167	1.003	1.007	1.014	1.001	1.003	1.002
1.062	1.205	1.280	1.041	1.022	1.061	1.001	1.003	1.003

Table 5: Composite curved panel: first 4 normalized buckling loads $[45, -45, 0]_s$ with C_2 interpolation.

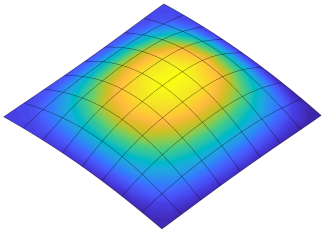

(a) mode 1 $[0]_6$

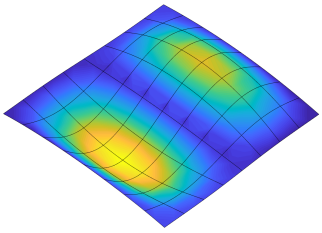

(c) mode 2 $[0]_6$

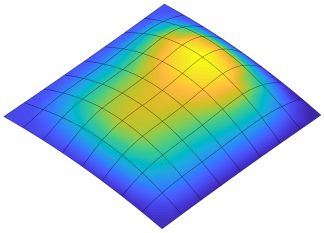

(b) mode 1 $[45/-45/0]_s$

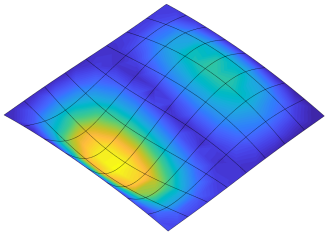

(d) mode 2 $[45/-45/0]_s$

Figure 2: Composite curved panel: first and second buckling mode for two layups

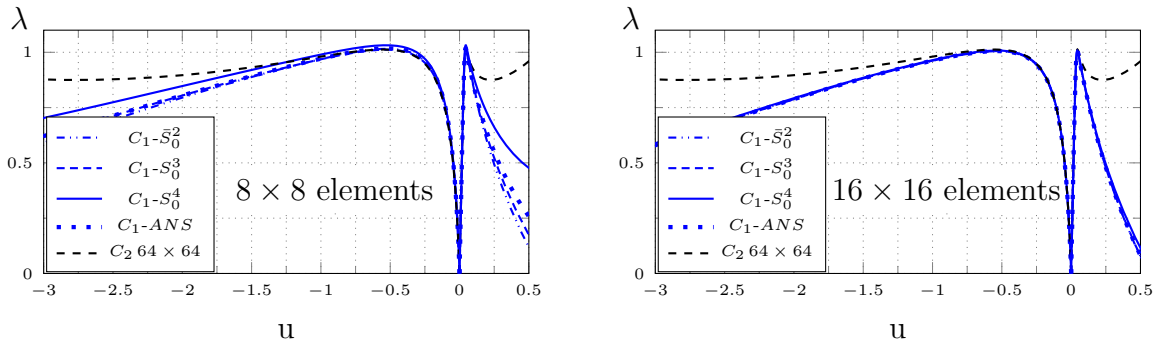

Figure 3: Composite curved panel: equilibrium path for $[0]_6$ and C_1 interpolation

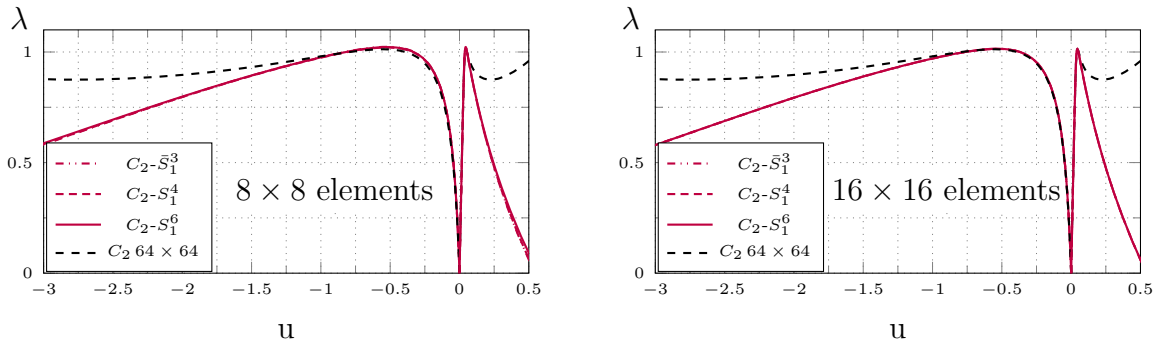

Figure 4: Composite curved panel: equilibrium path for $[0]_6$ and C_2 interpolation

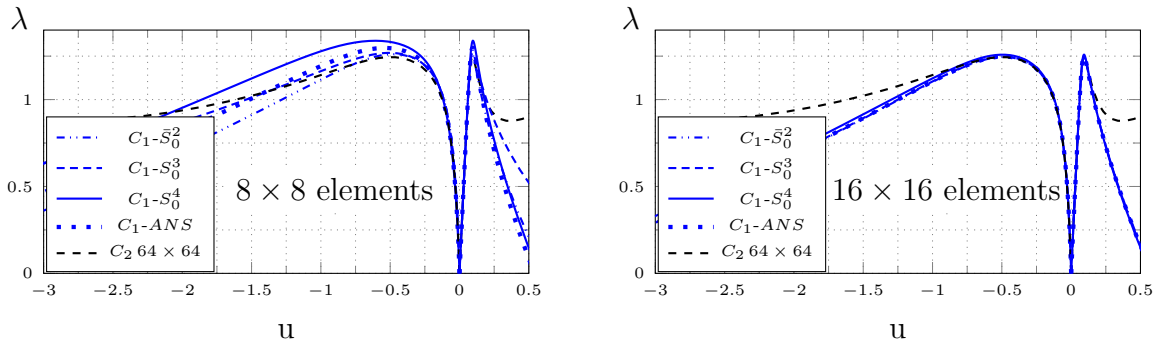

Figure 5: Composite curved panel: equilibrium path for $[45/-45/0]$ and C_1 interpolation

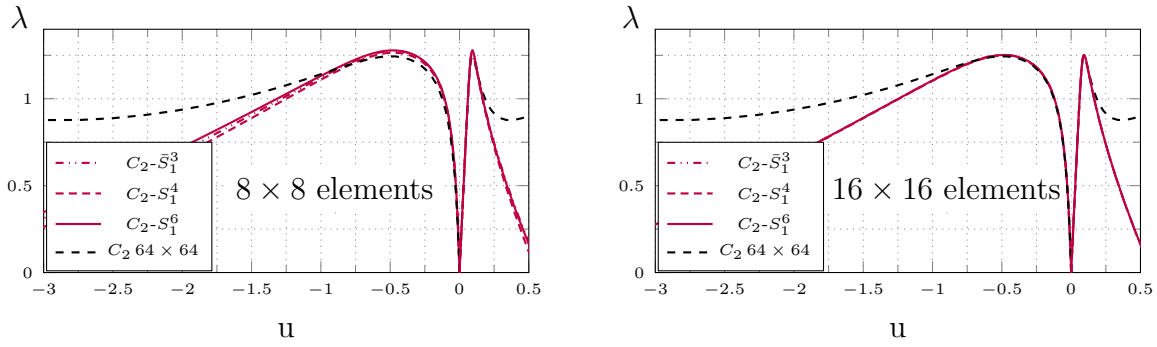

Figure 6: Composite curved panel: equilibrium path for $[45/-45/0]$ and C_2 interpolation

12 elm.				24 elm.				48 elm.			
$\bar{S}_0^2$	S_0^3	S_0^4	ANS	$\bar{S}_0^2$	S_0^3	S_0^4	ANS	$\bar{S}_0^2$	S_0^3	S_0^4	ANS
0.957	1.594	$*$	1.658	1.003	1.041	1.200	1.056	1.000	1.002	1.015	1.001
0.960	1.596	$*$	1.664	1.006	1.046	1.200	1.059	1.000	1.002	1.015	1.001
0.959	1.618	$*$	1.661	1.005	1.044	1.200	1.060	1.000	1.002	1.014	1.001
0.962	1.618	$*$	1.719	1.007	1.048	1.208	1.060	1.000	1.002	1.014	1.001

$* > 2$

Table 6: Laminate composite cylinder: first 4 normalized buckling loads for C_1.

12 elm.			24 elm.			48 elm.		
$\bar{S}_1^3$	S_1^4	S_1^6	$\bar{S}_1^3$	S_1^4	S_1^6	$\bar{S}_1^3$	S_1^4	S_1^6
1.156	1.120	1.245	1.003	1.011	1.007	1.000	1.001	1.000
1.176	1.127	1.245	1.003	1.011	1.007	1.000	1.001	1.000
1.175	1.150	1.266	1.002	1.012	1.006	1.000	1.001	1.000
1.183	1.150	1.278	1.002	1.012	1.006	1.000	1.001	1.000

Table 7: Laminate composite cylinder: first 4 normalized buckling loads for C_2.

3.2 Laminate composite cylinder subjected to axial compression

The cylinder considered in the following and labelled Z33 was manufactured and tested by DLR (German Aerospace Center). Geometry, material properties and boundary conditions are reported in [12]. The lowest buckling loads of the perfect structure are reported in Table 6 and Table 7 for the C_1 and the C_2 interpolation respectively. The corresponding buckling modes are depicted in Fig.7. Due to problem symmetries they occur in couples. Also for this test, C_1-$\bar{S}_0^2$, C_2-$\bar{S}_1^3$ and C_2-S_1^4 turn out to be particularly accurate and provide good results with a relatively coarse mesh in comparison with those usually employed in the FE literature [12]. In evaluating the initial post-buckling behavior a load imperfection is introduced by a concentrated force halfway up the cylinder axis. By including just one mode in the ROM, a good prediction of the limit load is obtained as shown in Fig.8 and Fig.7.

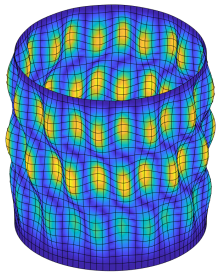

(a) mode 1 and mode 2

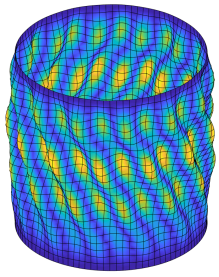

(b) mode 3 and mode 4

Figure 7: Laminate composite cylinder: first 4 buckling modes.

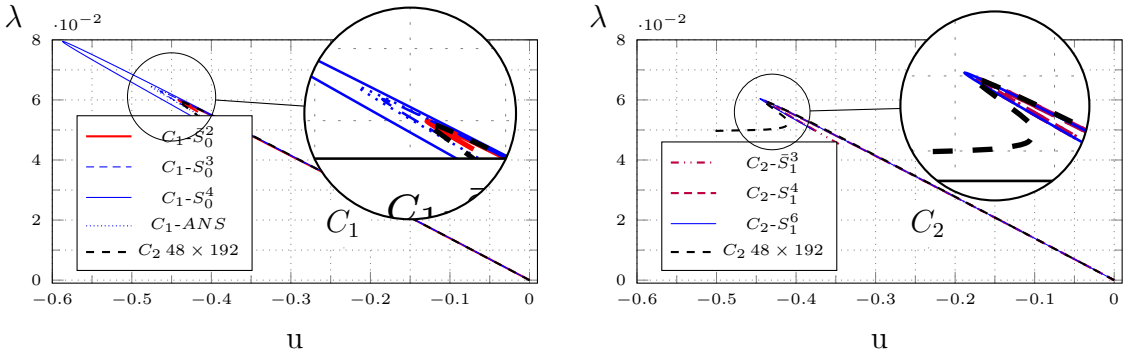

Figure 8: Laminate composite cylinder: equilibrium path using 24×96 mesh

4 CONCLUSIONS

This work explored the use of IGA for the construction of a reduced model for composite shells undergoing buckling. The results showed that the isogeometric model is able to furnish an excellent approximation of the buckling loads, the limit loads and the initial post-buckling behavior employing a very low number of DOFs and a reduced number of integration points. In particular the C_1-$\bar{S}_0^2$ and C_2-$\bar{S}_1^3$ approaches proves to be convenient because it requires just one integration point per element without spurious modes.

REFERENCES

[1] G. Garcea, F. S. Liguori, L. Leonetti, D. Magisano, A. Madeo, Accurate and efficient a posteriori account of geometrical imperfections in Koiter finite element analysis, International Journal for Numerical Methods in Engineering 112 (9) (2017) 1154–1174. doi:10.1002/nme.5550.

[2] D. Magisano, L. Leonetti, G. Garcea, Koiter asymptotic analysis of multilayered composite structures using mixed solid-shell finite elements, Composite Structures 154 (2016) 296–308. doi:10.1016/j.compstruct.2016.07.046.

[3] D. Magisano, L. Leonetti, G. Garcea, Advantages of the mixed format in geometrically nonlinear analysis of beams and shells using solid finite elements, International Journal for Numerical Methods in Engineering 109 (9) (2017) 1237–1262. doi:10.1002/nme.5322.

[4] K. Sze, W. Chan, T. Pian, An eight-node hybrid-stress solid-shell element for geometric non-linear analysis of elastic shells, International Journal for Numerical Methods in Engineering 55 (7) (2002) 853–878. doi:10.1002/nme.535.

[5] Y. B. J. Austin Cottrell, Thomas J. R Hughes, Isogeometric Analysis: Toward Integration of CAD and FEA, 2009. doi:978-0-470-74873-2.

[6] G. Garcea, R. Gonçalves, A. Bilotta, D. Manta, R. Bebiano, L. Leonetti, D. Magisano, D. Camotim, Deformation modes of thin-walled members: A comparison be-

tween the method of generalized eigenvectors and generalized beam theory, Thin-Walled Structures 100 (2016) 192–212. doi:10.1016/j.tws.2015.11.013.

[7] G. Garcea, L. Leonetti, D. Magisano, R. Gonçalves, D. Camotim, Deformation modes for the post-critical analysis of thin-walled compressed members by a Koiter semi-analytic approach, International Journal of Solids and Structures 110-111 (2017) 367–384. doi:10.1016/j.ijsolstr.2016.09.010.

[8] D. Magisano, L. Leonetti, G. Garcea, How to improve efficiency and robustness of the Newton method in geometrically non-linear structural problem discretized via displacement-based finite elements, Computer Methods in Applied Mechanics and Engineering 313 (2017) 986 – 1005. doi:http://dx.doi.org/10.1016/j.cma.2016.10.023.

[9] K. A. Johannessen, Optimal quadrature for univariate and tensor product splines, Computer Methods in Applied Mechanics and Engineering 316 (2017) 84 – 99, special Issue on Isogeometric Analysis: Progress and Challenges. doi:http://doi.org/10.1016/j.cma.2016.04.030.

[10] C. Adam, T. Hughes, S. Bouabdallah, M. Zarroug, H. Maitournam, Selective and reduced numerical integrations for NURBS-based isogeometric analysis, Computer Methods in Applied Mechanics and Engineering 284 (2015) 732–761. doi:10.1016/j.cma.2014.11.001.

[11] Leonardo Leonetti and Francesco Liguori and Domenico Magisano and Giovanni Garcea, An efficient isogeometric solid-shell formulation for geometrically nonlinear analysis of elastic shells, Computer Methods in Applied Mechanics and Engineering 331 (2018) 159 – 183. doi:https://doi.org/10.1016/j.cma.2017.11.025.

[12] Magisano, D. and Liang, K. and Garcea, G. and Leonetti, L. and Ruess, M., An efficient mixed variational reduced-order model formulation for nonlinear analyses of elastic shells, International Journal for Numerical Methods in Engineering 113 (4) (2018) 634–655. doi:10.1002/nme.5629.